RSC Advances

ROYAL SOCIETY OF CHEMISTRY

www.rsc.org/advances

Electrochemical and DFT study on the inhibition of 316L stainless steel corrosion in acidic medium by 1-(4-nitrophenyl)-5-amino-1*H*-tetrazole

Ali Ehsani[a*], Mohammad Ghasem Mahjani[b], Reza Moshrefi[b], Hossein Mostaanzadeh[b], Javad Shabani[b]

[a] *Department of Chemistry, Faculty of science, University of Qom, Qom, Iran*

[b] *Department of Chemistry, Faculty of science, K. N. Toosi University of Technology , Tehran, Iran*

*Corresponding author.

E-mail address:ehsani46847@yahoo.com & a.ehsani@qom.ac.ir (A. Ehsani)

Tel: (009825) 32103038

Fax: (009825) 32854973

Abstract

1-(4-nitrophenyl)-5-amino-1*H*-tetrazole was synthesized and its inhibiting action on the corrosion of stainless steel 316L stainless steel (SS) in sulfuric acid was investigated by means of potentiodynamic polarization and electrochemical impedance spectroscopy (EIS). In the potentiodynamic polarization measurements the values of βc had small changes with increasing inhibitor concentration, which indicated that the 1-(4-nitrophenyl)-5-amino-1*H*-tetrazole was adsorbed on the metal surface and the addition of the inhibitor hindered the acid attack on the SS electrode. The shift in the anodic Tafel slope βa might be attributed to the modification of anodic dissolution process due to the inhibitor modules adsorption on the active sites. The results of the investigation show that the newly synthesized compound show excellent inhibition efficiencies against the corrosion of SS in acidic solution. The adsorption of 1-(4-nitrophenyl)-5-amino-1*H*-tetrazole onto the SS surface followed the Langmuir adsorption model with the free energy of adsorption ΔG^{0}_{ads} of -9.44 kJ mol^{-1}. Quantum chemical calculations were employed to give further insight into the mechanism of inhibition action of 1-(4-nitrophenyl)-5-amino-1H-tetrazole.

Keywords: metal, corrosion test, electrochemical properties

1. Introduction

Stainless steels, especially austenite stainless steel, are widely applied in many fields because of their excellent corrosion resistance. The high corrosion resistance of austenitic stainless steel is primarily attributed to the passive film that consists of iron and chromium oxides and hydroxide- and water-containing compound. Type 316L stainless steel is widely used in the chemical, petrochemical and petroleum industries because of its good corrosion resistance, especially pitting resistance. One of most important tasks is the retardation of the attack by acid solutions used during pickling, industrial cleaning and descaling. The use of an additive is one of the major solutions for this problem. Hence, various additives are used to protect iron and its alloy against corrosive attack [1-5]. The use of organic molecules containing functional groups and p electrons in their structure, as corrosion inhibitors, is one of the most practical methods for protecting metals against corrosion and it is becoming increasingly popular. The existing data show that organic inhibitors act by adsorption and they protect the metal by film formation. Organic compounds bearing heteroatoms with high electron density such as phosphorus, sulfur, nitrogen, oxygen or those containing multiple bonds which are considered as adsorption centers, are effective as corrosion inhibitors [6-10]. The compounds containing both nitrogen and sulfur in their molecular structure have exhibited greater inhibition compared with those possessing only one of these atoms [11-13]. In the literature, many thiazole derivatives have been reported as corrosion inhibitors and found to have good corrosion inhibition effect [14,15]. Aminotetrazoles are important heterocyclic compounds from a biological point of view. It is known that they have applications in the pharmaceutical arena, as anticorrosive additives, as explosive and information recording systems, as ligands, and also as precursors to a variety of nitrogen-containing compounds. Aminotetrazoles have been reported as antiallergic and

antiasthmatic, antiviral and anti-inflammatory, antineoplastic, and to have cognition disorder activities [16, 17]. The choice of 1-(4-nitrophenyl)-5-amino-1*H*-tetrazole was based on the consideration that it contains good π-electron conjugation, enhancing its coordination, and an abundance of heteroatoms, enhancing its adsorption onto the surface of SS. The initial aim of the present investigation was to understand the inhibition properties of 1-(4-nitrophenyl)-5-amino-1*H*-tetrazole against SS corrosion in pickling acids and a proper understanding of the mechanism of inhibition. The inhibitor action of 1-(4-nitrophenyl)-5-amino-1*H*-tetrazole at different temperatures was followed by means of weight loss and electrochemical techniques such as Tafel polarization and electrochemical impedance spectroscopy. Quantum chemical calculations based on DFT method was performed on new compound used as corrosion inhibitor for SS in acid media to determine the optimized structural parameters, such as the frontier molecular orbital energy HOMO (highest occupied molecular orbital) and LUMO (lowest unoccupied molecular orbital) the charge distribution of the studied inhibitors, the absolute electronegativity (χ) values and the fraction of electrons (ΔN) transfer from inhibitors to SS.

2. Experimental

2.1. Materials and apparatus

316L Stainless steel has the composition (wt %) Fe: 67.95, Ni: 10.60, Si: 0.45, Mn: 1.75, Cr: 16.50, S: 0.025, P: 0.028, Mo: 2.10, Al: 0.008, Co: 0.16, Cu: 0.35, Nb: 0.01 and V: 0.02. The exposed surface of SS was ground with silicon carbide abrasive paper from 400 to 1200, degreased with absolute ethanol, rinsed in distilled water, and dried in warm air. The corrosive medium was 0.5 M H_2SO_4 solution prepared from analytical reagent grade 98% sulfuric acid and distilled water [15]. Synthesis of 1-(4-nitrophenyl)-5-amino-1*H*-tetrazole was prepared according

to the literature [16-28]. A mixture of the 4-nitrophenylcyanamide (2 mmol), NaN_3 (3 mmol), and $ZnCl_2$ (2 mmol) in H_2O (16 mL) was ultrasonicated for 15 h at 70-80 °C. The reaction mixture was cooled to 25 °C, the solid residue was filtered, washed with H_2O and treated with 3 M HCl (4 mL). The crude product was purified by aqueous ethanol to afford the pure product and characterized by ^{1}H NMR, ^{13}C NMR, FT-IR, elemental analysis (CHN), and melting points [17]. M.p. 187-188 °C; FT-IR (KBr, cm^{-1}): 3389, 3302, 3124, 1651, 1611, 1598, 1577, 1523, 1506, 1466, 1348, 1315, 1296, 1131, 1108, 1074, 867, 858, 751, 690, 588, 506, 449; ^{1}H NMR (500 MHz, DMSO-d_6): δ_H = 8.43 (d, J = 7.2 Hz, 2H), 7.91 (d, J = 7.2 Hz, 2H), 7.19 (s, 2H);^{13}C NMR (125 MHz, DMSO-d_6): δ_C = 154.9, 147.1, 138.6, 125.3, 124.6; CHN: Anal. Calcd for $C_7H_6N_6O_2$: C, 40.78; H, 2.93; N, 40.77; Found: C, 40.88; H, 3.01; N, 40.67.

The concentration range of 1-(4-nitrophenyl)-5-amino-1H-tetrazole) employed was 1×10^{-4} to 10^{-3} M in 0.5 M sulfuric acid. All electrochemical measurements were carried out in a conventional three electrode cell, powered by a potentiostat/galvanostat (EG&G 273A) and a frequency response analyzer (EG&G, 1025). The system was run by a PC through M270 and M398 software via a GPIB interface. The frequency range of 100 kHz to 100 mHz and modulation amplitude of 5 mV were employed for impedance studies at room temperature (298 k) .A saturated calomel electrode (SCE) and a platinum wire were used as reference and counter electrodes, respectively. Before measurement, the working electrode was immersed in test solution for approximately 1 h until a steady open circuit potential (OCP) was reached. The polarization curves were carried out from cathodic potential of -1.4 V to anodic potential of 0.10 V with respect to the open circuit potential at a sweep rate of 0.5 mV/s. The linear Tafel segments of the anodic and cathodic curves were extrapolated to corrosion potential (E_{corr}) to obtain the corrosion current densities (i_{corr}). In each measurement, a fresh working electrode was

used. Several runs were performed for each measurement to obtain reproducible data. The impedance and Tafel data were analyzed by Z-view (Scribner Associated Inc.) and powersuit software respectively.

2.2. Computational details

The use of quantum chemical calculations has become popular for screening new potential corrosion inhibitors [27]. Theoretical calculations were carried out at density functional theory (DFT) level using the 6-31*G* (d,p) basis set for all atoms with Gaussian 03 program package. Electronic properties such as highest occupied molecular orbital (HOMO) energy, lowest unoccupied molecular orbital (LUMO) energy and frontier molecular orbital coefficients have been calculated. The molecular sketches of all compounds were drawn using Gauss View 03 [28]. The natural bond orbital (NBO) analysis, suggested by Reed *et al*. [29,30], was applied to determine the atomic charges.

3. Results and discussion

3.1. Potentiodynamic polarization studies

Polarization measurements were carried out to get information regarding the kinetics of anodic and cathodic reactions. The potentiodynamic polarization curves for SS in 0.5 M H_2SO_4 solution in the absence and presence of different concentrations of the inhibitor molecules are shown in Fig. 1. The values of electrochemical kinetic parameters such as corrosion potential (E_{corr}), corrosion current density (I_{corr}) and Tafel slopes, determined from these by extrapolation method, are listed in Table 1. In corrosion, quantitative information on corrosion currents and corrosion

potentials can be extracted from the slope of the curves, using the Stern-Geary equation, as follows [31]:

$$i_{corr} = \frac{1}{2.303R_p}\left(\frac{\beta_a \times \beta_c}{\beta_a + \beta_c}\right) \quad (1)$$

i_{corr} is the corrosion current density in Amps/cm^2; R_p is the corrosion resistance in ohms cm^2; β_a is the anodic Tafel slope in Volts/decade or mV/decade of current density; β_c is the cathodic Tafel slope in Volts/decade or mV/decade of current density; the quantity, $\frac{\beta_a \times \beta_c}{\beta_a + \beta_c}$, is referred to as the Tafel constant. The corrosion inhibition efficiency was calculated using the relation:

$$\eta(\%) = 100\left(\frac{i^*_{corr} - i_{corr}}{i^*_{corr}}\right) \quad (2)$$

where i_{corr}* and i_{corr} are uninhibited and inhibited corrosion current densities, respectively, determined by extrapolation of Tafel lines in the corrosion potential. The corrosion rates ν (mm year^{-1}) from polarization were calculated using the following Equation:

$$\upsilon = \frac{i_{corr} \times t \times M}{F \times S \times d} \times 10$$

where t is the time (s), M is the equivalent molar weight of working electrode (g mol^{-1}), F is Faraday constant (96500 C. mol^{-1}), S is the surface area of electrode, d is the density of iron and the constant 10 is used to convert the unit cm to mm. The results are presented in Table 1. The inhibitor molecule first adsorbs on the SS surface and blocks the available reaction sites. As the concentration of the inhibitor increases, the linear polarization resistance (LPR) increases and corrosion rate (CR) decreases. The surface coverage increases with the inhibitor concentration and the formation of inhibitor film on the SS surface reduces the active surface area available for the attack of the corrosive medium and delays hydrogen evolution and metal dissolution [32]. In

the cathodic domain, as seen in Table 1, the values of βc show small changes with increasing inhibitor concentration, which indicates that the 1-(4-nitrophenyl)-5-amino-1H-tetrazole is adsorbed on the metal surface and the addition of the inhibitor hinders the acid attack on the SS electrode. In anodic domain, the value of βa decreases with the presence of 1-(4-nitrophenyl)-5-amino-1H-tetrazole. The shift in the anodic Tafel slope βa might be attributed to the modification of anodic dissolution process due to the inhibitor modules adsorption on the active sites. Compared to the absence of 1-(4-nitrophenyl)-5-amino-1H-tetrazole, the anodic curves of the working electrode in the acidic solution containing the 1-(4-nitrophenyl)-5-amino-1H-tetrazole clearly shifted to the direction of current reduction, as it could be observed from these polarization results; the inhibition efficiency increased with inhibitor concentration reaching a maximum value of 71% at 10^{-3} mol/L.

3.2. Electrochemical impedance spectroscopy

Electrochemical impedance spectroscopy is an excellent technique that has been used in understanding the mechanism of corrosion, passivation phenomena and charge transfer mechanism in the electrolyte/electrode interface. This has been broadly discussed in the literature using a variety of theoretical models [33-37]. In this study, impedance measurements were performed under potentiostatic conditions after 1 h of immersion. Nyquist plots of uninhibited and inhibited solutions containing different concentrations of inhibitor molecules were performed over the frequency range from 100 mHz to 100 MHz and are shown in Fig. 2. The similarity in the shapes of these graphs throughout the experiment indicates that the addition of inhibitor molecules does not cause any noticeable change in the corrosion mechanism [32]. The Nyquist diagrams show one capacitive loop at high frequencies. The capacitive loop at high

frequencies represents the phenomenon associated with the electrical double layer. The above impedance diagrams (Nyquist) contain depressed semicircles with the centre under the real axis. Such behavior is characteristic of solid electrodes and often referred to as frequency dispersion, attributed to different physical phenomena such as roughness, inhomogeneities of the solid surfaces, impurities, grain boundaries, and distribution of surface active sites. The ideal capacitive behavior is not observed in this case and hence a constant phase element CPE is introduced in the circuit to give a more accurate fit [46-48]. The mechanism of corrosion remains unaffected during the addition of inhibitor molecules. The simplest fitting is represented by Randle's equivalent circuit (Fig. 2), which is a parallel combination of the charge transfer resistance (R_{ct}) and the constant phase element (CPE), both in series with the solution resistance (R_s). The impedance function of a CPE can be represented as [41]:

$$Z_{CPE} = Y_0^{-1}(j\omega)^{-n} \qquad (3)$$

where Y_0 is the CPE constant, ω is the angular frequency, and n is the CPE exponent, which can be used as a gauge of the heterogeneity or roughness of the surface [35,36]. In the present work, the value of n has a tendency to decrease with increasing inhibitor concentration, which may be attributed to the increase of inhibitor concentration resulted in the increasing surface roughness.

As seen in Table 2, Y_0 decreases with increase in concentration. This can be attributed to the gradual replacement of water molecules by the adsorption of the organic molecules at metal/solution interface, which is leading to a protective film on metal surface. The equation used for calculating the percentage inhibition efficiency is:

$$\eta(\%) = 100\left(\frac{R_{ct}^{*} - R_{ct}}{R_{ct}^{*}}\right) \qquad (4)$$

where R_{ct}^{*} and R_{ct} are values of the charge transfer resistance observed in the presence and absence of inhibitor molecules. Impedance parameters are summarized in Table 2. The results

obtained from the EIS technique in acidic solution were in good agreement with those obtained from the polarization method. As observed in Table 2, the adsorption of 1-(4-nitrophenyl)-5-amino-1H-tetrazole molecules on SS surface modifies the interface between the corrosive medium and metal surface and decreases its electrical capacity. The increase in R_{ct} values with increase in 1-(4-nitrophenyl)-5-amino-1H-tetrazole concentration can be interpreted as the formation of an insulated adsorption layer. At the highest inhibitor concentration of 10^{-3} mol/L, the inhibition efficiency increases and reaches 75.05%. Thus, it can be deduced that 1-(4-nitrophenyl)-5-amino-1H-tetrazole has a clear role in metal protection at the concentration of 10^{-3} M.

3.3. Weight Loss Measurements.

At different temperatures (298-318 K), the results of weight loss measurements in 0.5 M H_2SO_4 solution without and with different concentrations of 1-(4-nitrophenyl)-5-amino-1H-tetrazole are shown in Table 3. The corrosion rate of SS was determined using the relation

$$W = \frac{\Delta m}{St} \qquad (5)$$

where Δm is the mass loss, S the area and t is the immersion period. The inhibition efficiencies, $IE(\%)$, were calculated by the following equation:

$$IE(\%) = (\frac{W_0 - W}{W_0}) \times 100 \qquad (6)$$

W_0 and W are the corrosion rates in the absence and presence of the inhibitors, respectively. From Table 3, it can be found that as temperature increases, the corrosion rate improves and IE (%) reduces. This phenomenon might be attributed to the fact that higher temperature could speed up hot movement of the organic molecules and weaken the adsorption ability of inhibitor

on metal surface [34]. It can also be seen in Table 3 that the increase in inhibitor concentration leads to an increase in inhibition efficiency and a decrease in corrosion rate. This result suggests that plenty of adsorbed inhibitor molecules move onto the metal surface. Then, the contact area between metal surface and aggressive solution becomes smaller and smaller leading to the decrease in active sites. The inhibition efficiency obtained by weight loss measurements is lower than that from electrochemical experiments. This difference is attributed to weight loss experiments giving average corrosion rates, whereas the electrochemical experiments give instantaneous corrosion rates. Therefore, the discrepancy in inhibition efficiency obtained by the two methods is understandable. However, the trend in inhibition efficiency with increasing inhibitor concentration is similar regardless of the selection of electrochemical or weight loss method. The inhibition efficiency increases as inhibitor concentration increases.

3.4. Adsorption Isotherms.

The adsorption of an organic adsorbate at metal/solution interface can be presented as a substitution adsorption process between the organic molecules in aqueous solution, (Org_{aq}), and the water molecules on metallic surface, (H_2O_{ads}) Org_{aq}

$$Org_{aq} + XH_2O_{ads} \leftrightarrow Org_{ads} + XH_2O_{aq} \qquad (7)$$

where X, the size ratio, is the number of water molecules displaced by one molecule of organic inhibitor. X is assumed to be independent of coverage or charge on the electrode [47]. Basic information on the interaction between the inhibitors and the steel surface is provided by the adsorption isotherm. The degree of surface coverage, θ, at different inhibitor concentrations in 0.5 M H_2SO_4 was evaluated from weight loss measurements (θ = IE(%)/100) at 25 °C. The plot of C/θ against inhibitor concentration, C, displayed a straight line for the tested inhibitor (Fig.

3). The linear plot clearly revealed that the surface adsorption process of 1-(4-nitrophenyl)-5-amino-1H-tetrazole on the SS surface obeys the Langmuir isotherm. Likewise, it suggests that an adsorption process occurs, which can be expressed as follows [32]:

$$\frac{C}{\theta} = \frac{1}{K_{ads}} + C \qquad (8)$$

where K_{ads} is the equilibrium constant of the adsorption process. Free energy of adsorption (ΔG_{ads}) can be calculated by Eq. (9). The numeral of 51.45 is the molar concentration of water in the solution:

$$K_{ads} = \frac{1}{55.5}\exp\left(\frac{-\Delta G^{0}_{ads}}{RT}\right) \qquad (10)$$

The value of ΔG^0 ads for adsorption of 1-(4-nitrophenyl)-5-amino-1H-tetrazole was found to be -9.44kJ mol^{-1}. The negative value of ΔG^0 ads suggests that 1-(4-nitrophenyl)-5-amino-1H-tetrazole is spontaneously adsorbed on the SS surface. Literature survey reveals that the values of ΔG^0 ads around -20 kJ mol^{-1} or lower are consistent with the electrostatic interaction between the charged molecules and the charged metal (physical adsorption) [48].The adsorption of an inhibitor on the metal surface can occur on the basis of donor–acceptor interactions between the p-electrons of the heterocyclic compound and the vacant d-orbitals of the metal surface atoms. Therefore, the energies of the frontier orbitals should be considered. Energy of LUMO shows the ability of the molecule to receive charge when attacked by electron pair donors, even as the energy of HOMO to donate the charge when attached by electron seeking reagents. As the energy gap between the frontier orbitals gets smaller, the interactions between the reacting species strengthen. In this regard, the electronic properties such as highest occupied molecular orbital (HOMO) energy, lowest unoccupied molecular orbital (LUMO) energy and frontier molecular orbital coefficients have been calculated for prepared inhibitor. The natural bond

orbital (NBO) analysis was applied to determine the atomic charges. Results are presented in Figure 4 and tables 4, 5, 6. According to the results, HOMO location in the 1-(4-nitrophenyl)-5-amino-1H-tetrazole molecule is mostly distributed in the vicinity of the nitrogen atoms. This indicates the reactive sites of the interaction between 1-(4-nitrophenyl)-5-amino-1H-tetrazole and the SS surface. Mulliken population analysis, presented in Fig. 4e, is further evidence for the interaction between SS surface and inhibitor active sites. It is clear from figure 4 that the nitrogen atoms of 1-(4-nitrophenyl)-5-amino-1H-tetrazole have considerable excess of negative charge than other atoms. Thus, the adsorption of 1-(4-nitrophenyl)-5-amino-1H-tetrazole as a neutral molecule on the metal surface can occur directly involving the displacement of water molecules from the metal surface and sharing of electrons between the nitrogen atoms and the metal surface. It should be noted that 1-(4-nitrophenyl)-5-amino-1H-tetrazole adsorbs mainly through electrostatic interactions between the positively charged nitrogen atom (since acidic solution can protonate the nitrogen atoms of 1-(4-nitrophenyl)-5-amino-1H-tetrazole and the negatively charged metal surface (physisorption) as evident in the value of ΔG^0_{ads} obtained.

4. Conclusion

1-(4-nitrophenyl)-5-amino-1H-tetrazole was found to inhibit the corrosion of SS in 0.5 M H_2SO_4 solution and the extent of inhibition was concentration dependent. Inhibition efficiency increases with increasing inhibitor concentration. EIS plots indicate that the charge transfer resistances increase with increasing concentration of the inhibitor at the highest inhibitor concentration of 10^{-3} mol/L, the inhibition efficiency increases. 1-(4-nitrophenyl)-5-amino-1H-tetrazole inhibits corrosion by getting adsorbed on the metal surface following Langmuir

adsorption isotherm. Quantum chemical calculations show that the adsorption sites are mainly located around the nitrogen atoms of 1-(4-nitrophenyl)-5-amino-1H-tetrazole.

Acknowledgements

We gratefully acknowledge the support of this work by Qom University and K. N. Toosi University of Technology Research Councils.

References

[1] I. Ahamad, M.A. Quraishi, *Corros. Sci*, 2009, **51**, 2006-2013.

[2] Q.B. Zhang, Y.X. Hua, *Electrochim. Acta* , 2009, **54** , 1881-1887.

[3] W. Li, Q. He, C. Pei, B. Hou, *Electrochim. Acta*, 2007, **52,** 6386-6394.

[4] R. Solmaz, G. Kardas, B. Yazıcı, M. Erbil, *Prot. Met*, 2005, **41**, 581-585.

[5] G. Kardas, *Mater. Sci*, 2005, **41**, 337-343.

[6] J. Aljourani, K. Raeissi, M.A. Golozar, *Corros. Sci*, 2009, **51**, 1836-1843.

[7] M.L. Zheludkevich, K.A. Yasakau, S.K. Poznyak, M.G.S. Ferreira, *Corros. Sci*, 2005, **47**, 3368-3383.

[8] I.B. Obot, N.O. Obi-Egbedi, S.A. Umoren, *Corros. Sci*, 2009, **51**, 276-282.

[9] M.G. Hosseini, M. Ehteshamzadeh, T. Shahrabi, *Electrochim. Acta*, 2007, **52**, 3680-3685.

[10] S. Afak, B, Duran, A. Yurt, G. Turkoglu, *Corros. Sci*, 2012, **54**, 251-259.

[11] H.H. Hassan, E. Adbelghani, M.A. Amin, *Electrochim. Acta,* 2007, **52,** 6359-6366.

[12] Y. Abdoud, A. Abourrriche, T. Saffaj, M. Berrada, M. Charrouf, A. Bennamara, N. Al Himidi, H. Hannache*, Mater. Chem. Phys*, 2007, **105,** 1-5.

[13] M.A. Quaraishi, J. Rawat, M. Ajmal, *J. Appl. Electrochem*, 2000, **30**, 745-751.

[14] K.F. Khaled, M.A. Amin, *Corros. Sci*, 2009, **51**, 1964-1975.

[15] S. Safak B. Duran , A, Yurt, G. Turkoglu, *Corros. Sci* , 2012, **54**, 251–259.

[16] D. Habibi, M. Nasrollahzadeh, H. Sahebekhtiari, R.V. Parish, *Tetrahedron*, 2013, **69**, 3082-3087.

[17] D. Habibi, M. Nasrollahzadeh, H. Sahebekhtiari. S.M. Sajadi, *Synlett*, 2012, **23**, 2795–2798.

[18] A.R. Modarresi-Alam, F. Khamooshi, M. Rostamizadeh, H. Keykha, M. Nasrollahzadeh, H.R. Bijanzadeh, E.J. Kleinpeter, *Mol. Struc*, 2007, **841**, 61-66.

[19] H. Shahroosvand, L. Najafi, E. Mohajerani, A. Khabbazi, M. Nasrollahzadeh, *J. Mater Chem. C*, 2013, **1,** 1337-1344.

[20] H. Shahroosvand, L. Najafi, E. Mohajerani, M. Janghouri, M. Nasrollahzadeh, *RSC Adv*, 2013, **3,** 6323-6326.

[21] A.R. Modarresi-Alam, M. Nasrollahzadeh,*Turk. J. Chem*, 2009, **33** , 267-280.

[22] D. Habibi, M. Nasrollahzadeh, L. Mehrabi, S. Mostafaee, *Monatsh. Chem*, 2013, **144**, 725-728.

[23] D. Habibi, M. Nasrollahzadeh, Y. Bayat. *Synth. Commun*, 2011, **41** ,2304.

[24] D. Habibi, M. Nasrollahzadeh. *Synth. Commun*,2012, **42** , 2023-2032.

[25]D. Habibi, M. Nasrollahzadeh, *Synth. Commun*, 2010, **40**, 3159-3167.

[26] M. Nasrollahzadeh, D. Habibi, Z. Shahkarami, Y. Bayat, *Tetrahedron*, 2009, **65,** 10715-10719.

[27] D. Habibi, M. Nasrollahzadeh, A.R. Faraji, Y. Bayat, *Tetrahedron*, 2010, **66,** 3866-3870.

[28] M. Nasrollahzadeh, A. Ehsani, M. Maham, *Synlett*, 2014, **25**, 505-508.

[29] A. Kokalj, *Electrochim. Acta, 2010*, **56,** 745-755.

[30] Gauss View, Version 3.0, Gaussian Inc., Pittsburgh, PA, 2003.

[31] A.E. Reed, F. Weinhold, *Chem. Rev*. 1998, **88**, 899-926.

[32] H.B. Schelegel, Ab Initio Methods in Quantum Chemistry, John Wiley, New York, 1987. pp. 249-286.

[33] M.G. Mahjani, R. Moshrefi, A. Ehsani, M. Jafarian, *Anti- corrosion methods and materials*, 2011, **58**, 250-257.

[34] T. Zhihua, Z. Shengtao, L. Weihua, H. Baorong, *Ind. Eng. Chem. Res* , 2011, **50** 6082-6088.

[35] A. Ehsani, M.G. Mahjani, M. Jafarian, *Turk. J. Chem*, 2011, **35***,* 1-9.

[36] A. Ehsani, F. Babaei, M. Nasrollahzadeh, *Appl. Surf. Sci.* 2013, **283**, 1060-1064.

[37] A. Ehsani, M. G. Mahjani, M. Jafarian, A. Naeemy, *Electrochim. Acta* , 2012, **71,** 128-133.

[38] A. Ehsani, M.G. Mahjani,M. Jafarian, A. Naeemy, *Prog. Org. Coat*, 2010, **69**, 510-516.

[39] A. Ehsani, M.G. Mahjani, M. Jafarian, *Synth. Met*, 2011, **161**, 1760-1765.

[40] A. Ehsani, B. Jaleh, M. Nasrollahzadeh, *J. Power. Sources*, 2014, **257,** 300-307.

[41]A. Ehsani, M. Nasrollahzadeh, MG. Mahjani, R. Moshrefi, H. Mostaanzadeh , *J. Ind. Eng. Chem*, doi: 10.1016/j.jiec.2014.01.045.

[42] **A.** Ehsani, S. Adeli, F. Babaei, H. Mostaanzadeh, M. Nasrollahzadeh, *J. Electroanal. Chem*. 2014, **713**, 91–97.

[43] A. Ehsani, M.G. Mahjani, M. Bordbar, S. Adeli, *J. Electroanal. Chem*. 2013, **710**, 29-35.

[44] M. G. Mahjani, A. Ehsani, M. Jafarian, *Synth. Met*, 2010, **160**, 1252–1258.

[45] A. Ehsani, M.G. Mahjani, M. Jafarian, *Synth. Met*, 2012, **62**, 199-204.

[46] H. Hassan, *Electrochim. Acta,* 2006*,* **51**, 5966-5972.

[47] S. Martinez, *Mater. Chem. Phys*, 2002, **77**, 97-102.

[48] P. Hohenberg, W. Kohn, *Phys. Rev. A*, 1964, **136**, 864.

Figures and tables captions

Fig. 1. Potentiodynamic polarisation curves of SS in 0.5 M H_2SO_4 solution in the absence and presence of various concentrations of the 1-(4-nitrophenyl)-5-amino-1H-tetrazole.

Fig. 2. Nyquist plots of SS in 0.5 M H_2SO_4 solution containing different concentrations of the 1-(4-nitrophenyl)-5-amino-1H-tetrazole. Electrical equivalent circuit used for modeling metal/solution interface in the absence and presence of inhibitors.

Fig. 3. Langmuir adsorption plot for SS in 0.5 M H_2SO_4 containing different concentrations of 1-(4-nitrophenyl)-5-amino-1H-tetrazole.

Fig. 4. (a) Structure of 1-(4-nitrophenyl)-5-amino-1H-tetrazole; (b) Optimized molecular structure of 1-(4-nitrophenyl)-5-amino-1H-tetrazole, H atoms have been omitted for clarity; (c) The highest occupied molecular orbital (HOMO) of 1-(4-nitrophenyl)-5-amino-1H-tetrazole; (d) The lowest unoccupied molecular orbital (LUMO) of 1-(4-nitrophenyl)-5-amino-1H-tetrazole; (e) Muliken charge population analysis and vector of dipole moment of 1-(4-nitrophenyl)-5-amino-1H-tetrazole; (f) Natural charge population analysis of 1-(4-nitrophenyl)-5-amino-1H-tetrazole and.

Table 1. Corrosion parameters obtained from Tafel polarisation curves of SS in 0.5M H_2SO_4 in the absence and presence of different concentrations of 1-(4-nitrophenyl)-5-amino-1H-tetrazole at 298 K.

Table 2. Impedance parameters for the corrosion of SS in 0.5M H_2SO_4 containing different concentration of 1-(4-nitrophenyl)-5-amino-1H-tetrazole at 298 K.

Table 3. Results of weight loss test and IE_w% of 1-(4-nitrophenyl)-5-amino-1H-tetrazole inhibitor with different concentration and different temperature in 0.5 M H_2SO_4.

Table 4. Orbital energies for HOMO, LUMO, HOMO-LUMO gap energy (ΔE) and dipole moment (μ) of Compound in the gaseous phase. All quantum chemical parameters calculated at DFT level using the 6-31G(d,p) basis set.

Table 5. Electronegativity (χ), global hardness (η) and proportion of electrons transferred (ΔN) of 1-(4-nitrophenyl)-5-amino-1H-tetrazole.

Table 6. Muliken and Natural Charges (e) for atoms in 1-(4-nitrophenyl)-5-amino-1H-tetrazole.

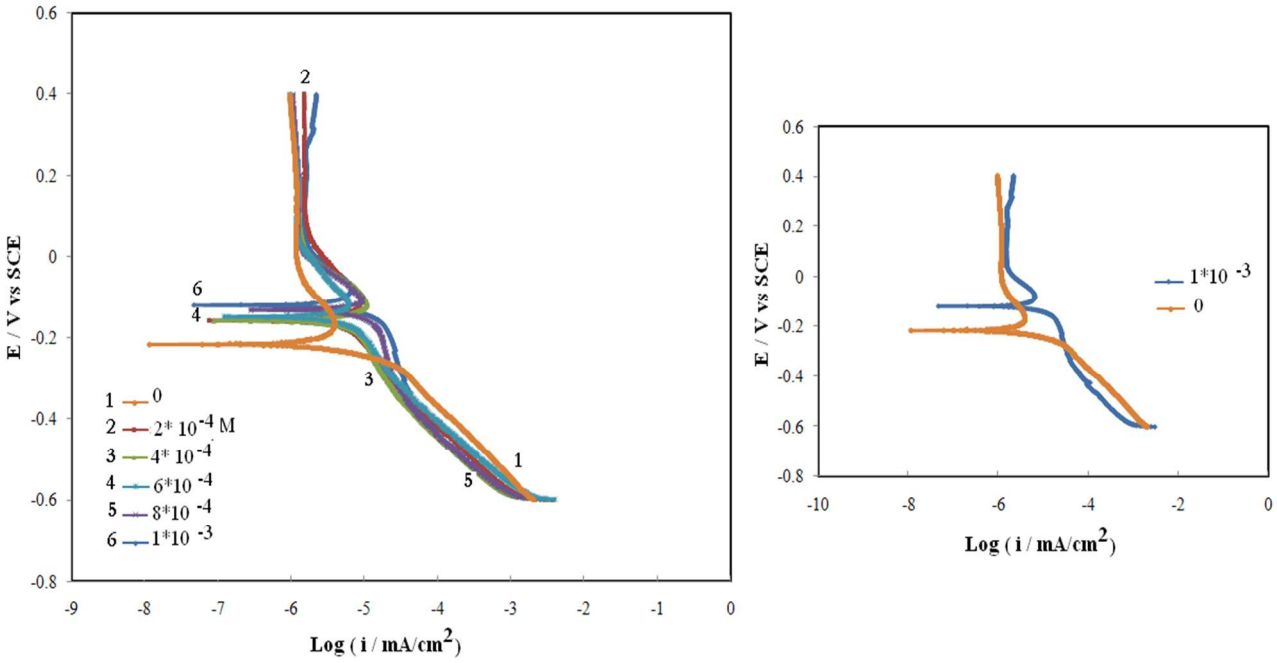

Figure 1.

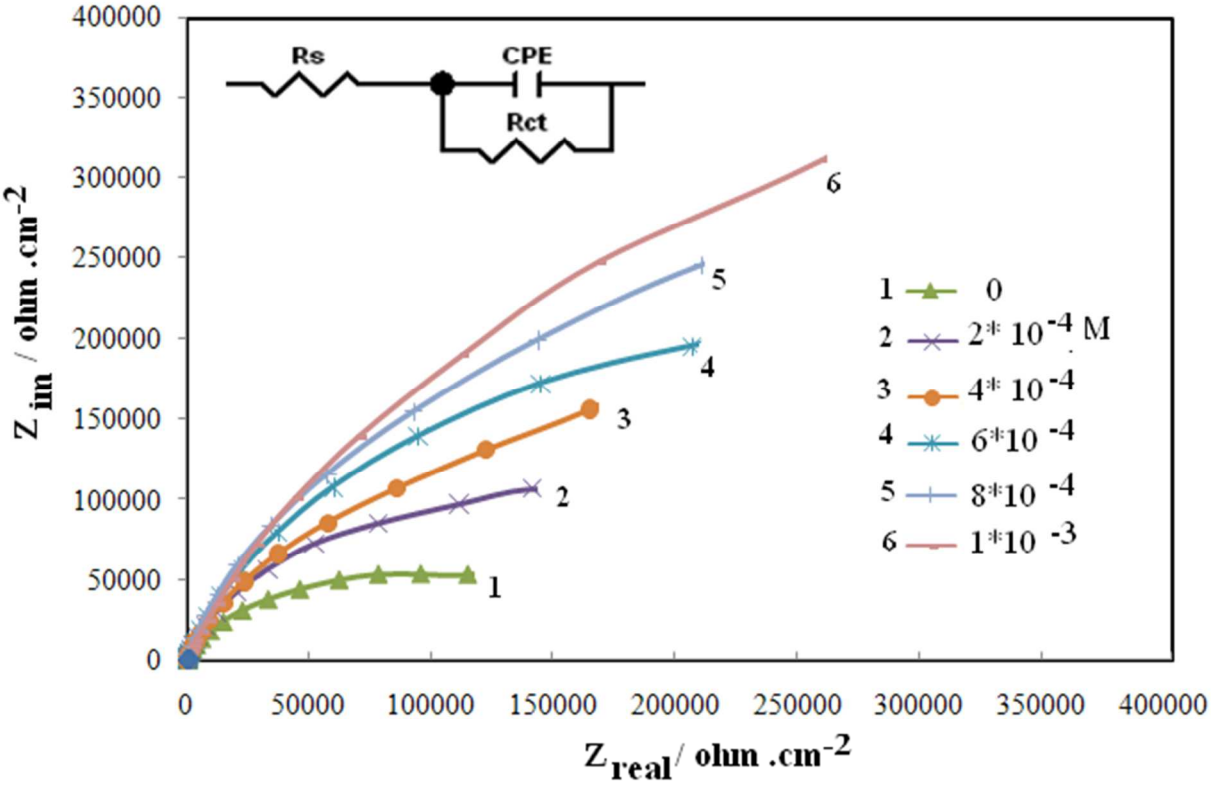

Figure 2.

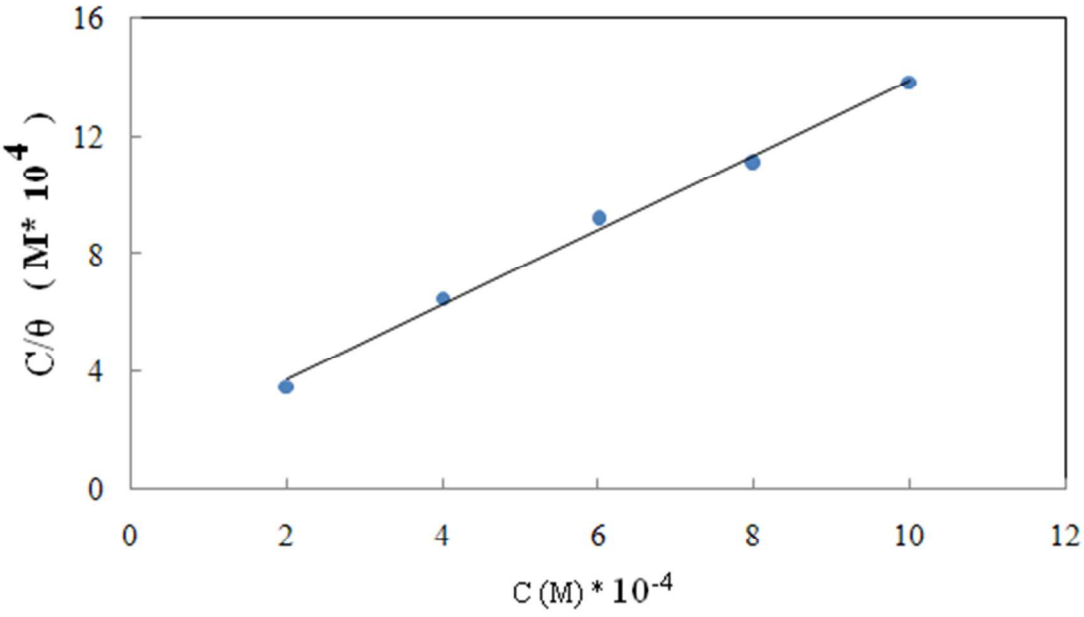

Figure 3.

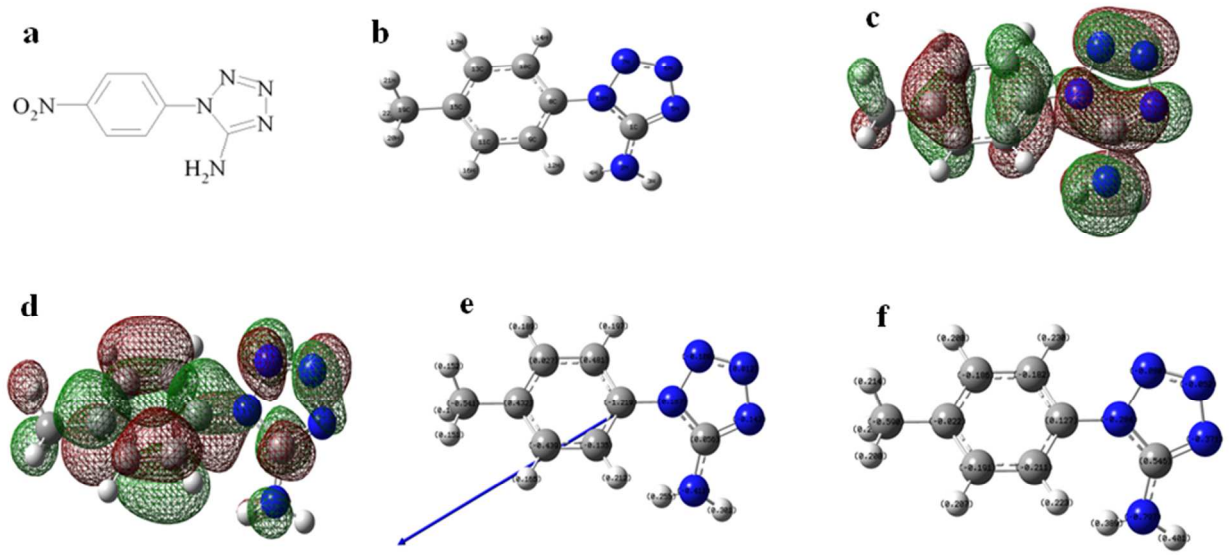

Figure 4.

Table 1: Corrosion parameters obtained from Tafel polarisation curves of SS 316L in 0.5M H_2SO_4 in the absence and presence of different concentrations of 1-(4-nitrophenyl)-5-amino-1H-tetrazole at 298 K.

No.	Inhi. Con.	Ba(v/decade)	Bc(v/dedade)	I(uA)	E(v)	CR(mpy)
SS1	0	0.61	0.14	12.76	-0.22	5.25
SS2	0.0001	0.058	0.23	5.98	-0.14	2.46
SS3	0.0002	0.026	0.20	5.40	-0.16	2.21
SS4	0.0004	0.036	0.20	4.887	-0.16	2.01
SS5	0.0006	0.038	0.23	4.21	-0.13	1.73
SS6	0.0008	0.041	0.19	4.014	-0.16	1.687
SS7	0.001	0.010	0.20	3.697	-0.12	1.52

Table 2. Impedance parameters for the corrosion of SS in 0.5M H_2SO_4 containing different concentration of 1-(4-nitrophenyl)-5-amino-1H-tetrazole at 298 K.

Concentration x (M)	R_s ($\Omega\,cm^2$)	Y_0 ($\mu\Omega^{-1}s^n cm^{-2}$)	n	R_{ct} ($k\Omega\,cm^2$)	IE%
0	4.25	152.85	0.89	12.35	
2.0×10^{-4}	7.61	144.17	0.87	23.87	48.26
4.0×10^{-4}	8.36	105.61	0.84	28.19	56.19
6.0×10^{-4}	8.56	83.18	0.84	34.12	63.80
8.0×10^{-4}	9.24	73.15	0.80	42.76	71.11
1.0×10^{-3}	9.48	54.32	0.76	49.51	75.05

Table 3: Results of weight loss test and IE_w% of 1-(4-nitrophenyl)-5-amino-1H-tetrazole inhibitor with different concentration and different temperature in 0.5 M H_2SO_4

Inhibitor concentration (M)	Corrosion rate(mg cm^{-2} h^{-1}) (298K)	IE_w %	Corrosion rate(mg cm^{-2} h^{-1}) (308K)	IE_w%	Corrosion rate(mg cm^{-2} h^{-1}) (318K)	IE_w%
0	5.16		7.87		10.12	
2.0×10^{-4}	2.25	57.05	3.58	54.51	5.12	49.40
4.0×10^{-4}	2.02	60.85	3.28	58.32	4.76	52.96
6.0×10^{-4}	1.78	65.50	2.89	63.27	4.18	58.69
8.0×10^{-4}	1.52	70.54	2.47	68.61	3.74	63.04
1.0×10^{-3}	1.21	76.50	2.22	71.79	3.52	65.21

Table 4. Orbital energies for HOMO, LUMO, HOMO-LUMO gap energy (ΔE) and dipole moment (μ) of 1-(4-nitrophenyl)-5-amino-1H-tetrazole in the gaseous (G) and aqueous (A) phases*.

phase	E_{HOMO}(ev)	E_{LUMO}(ev)	ΔE(ev)	μ(D)
G	-6.955	-1.355	5.600	7.3409
A	-6.973	-1.220	5.753	10.0942

*All quantum chemical parameters calculated at DFT level using the 6-31G(d,p) basis set.

Table 5. Electronegativity (χ), global hardness (η) and proportion of electrons transferred (ΔN) of 1-(4-nitrophenyl)-5-amino-1H-tetrazole.

phase	χ	η	ΔN
G	4.155	2.800	0.508
A	4.096	2.876	0.505

Table 6. Muliken and Natural Charges (e) for atoms in 1-(4-nitrophenyl)-5-amino-1H-tetrazole.

Atom	2N	5N	6 N	7 N	18 N
Muliken	-0.411	-0.142	0.012	-0.100	0.187
Natural	-0.797	-0.371	-0.052	-0.080	-0.284

This article describes the best corrosion inhibition behavior and adsorption of new synthesized amino tetrazole using electrochemical and computational methods.